ASMS

RESEARCH ARTICLE

Critical Evaluation of Kinetic Method Measurements: Possible Origins of Nonlinear Effects

Sandrine Bourgoin-Voillard,[1,5] Carlos Afonso,[1,2] Denis Lesage,[1] Emilie-Laure Zins,[3] Jean-Claude Tabet,[1] P. B. Armentrout[4]

[1]Institut Parisien de Chimie Moléculaire, UMR CNRS 7201, Université Pierre et Marie Curie-Paris6, Paris, France
[2]UMR CNRS 6014 COBRA, Université de Rouen, INSA de Rouen, Mont-Saint-Aignan, France
[3]Laboratoire de Dynamique, Interactions et Réactivité, LADIR, UMR 7075, CNRS, Université Pierre et Marie Curie-Paris6, Paris, France
[4]Department of Chemistry, University of Utah, Salt Lake City, UT 84112, USA
[5]*Present Address:* Cibles diagnostiques ou thérapeutiques et vectorisation de drogues dans le cancer du poumon INSERM U823, Institut Albert Bonniot, Université Joseph Fourier Plate-forme de Protéomique Prométhée, Institut de Biologie et Pathologie, CHU de Grenoble BP217, 38043 Grenoble Cedex 9, France
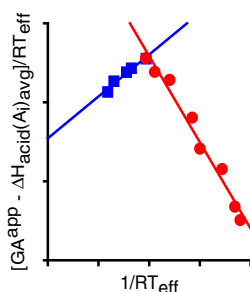
Abstract. The kinetic method is a widely used approach for the determination of thermochemical data such as proton affinities (PA) and gas-phase acidities ($\Delta H°_{acid}$). These data are easily obtained from decompositions of noncovalent heterodimers if care is taken in the choice of the method, references used, and experimental conditions. Previously, several papers have focused on theoretical considerations concerning the nature of the references. Few investigations have been devoted to conditions required to validate the quality of the experimental results. In the present work, we are interested in rationalizing the origin of nonlinear effects that can be obtained with the kinetic method. It is shown that such deviations result from intrinsic properties of the systems investigated but can also be enhanced by artifacts resulting from experimental issues. Overall, it is shown that orthogonal distance regression (ODR) analysis of kinetic method data provides the optimum way of acquiring accurate thermodynamic information.

Key words: Collision-induced dissociation, Energy-resolved MS, Entropy effects, Kinetic method
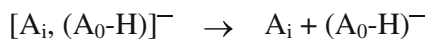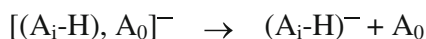
Introduction

The original Cooks' kinetic method was a landmark for comparison of thermochemical data by tandem mass spectrometry [1–4]. It constitutes a simple approach for the determination of thermochemical data such as proton affinities (PA) and gas-phase acidities ($\Delta H°_{acid}$). Such data for functionalized compounds (A_0) are obtained relative to reference compounds (A_i) with known PA or $\Delta H°_{acid}$ values. In the following discussion, only equations corresponding to acidity measurements will be considered, but are easily generalized. The method is based on the competitive dissociations of heterodimers (Scheme 1).

Correspondence to: P. B. Armentrout; *e-mail:* armentrout@chem.utah.edu

Originally, the method was applied to compounds presenting the same chemical function and thus entropic effects were limited. This standard Cooks' method is generally usable when (1) A_0 and A_i are mono-functional compounds, (2) the isomeric dimers [(A_0-H), A_i]$^-$ and [A_0, (A_i-H)]$^-$ are interconvertible (i.e., there is a low energy barrier between them), (3) T_{eff} is the same (or very close) for each dissociative heterodimer used for the $\Delta H°_{acid}(A_0)$ determination, and (4) the entropy variation associated with proton transfer is negligible [$\Delta\Delta S°_{acid}(A_0, A_i) \approx 0$]. According to the latter requirement, structural and physicochemical similarities for A_0 and A_i appear to be necessary. This last condition limits the choice of reference compounds. Fenselau and coworkers proposed an extended approach using references that are similar between themselves but different from the studied compounds [5]. In this case, entropic effects are considered as constant, $\Delta\Delta S°_{acid}(A_0, A_i) \approx$ constant. In theory, this constant could hold any value, however, it has been found that when the entropy variation difference between analyte and reference is too large ($\Delta\Delta S°_{acid}$ is greater

$$[(A_i\text{-}H), A_0]^- \rightarrow (A_i\text{-}H)^- + A_0$$

$$\downarrow\uparrow$$

$$[A_i, (A_0\text{-}H)]^- \rightarrow A_i + (A_0\text{-}H)^-$$

Scheme 1.

than 35–40 $J\,mol^{-1}\,K^{-1}$), the kinetic method does systematically under- or overestimate $\Delta H°_{acid}$ and $\Delta\Delta S°_{acid}$ [6, 7].

In the extended approach, experiments must be carried out under different activation conditions yielding changes in effective temperature in order to obtain the $\Delta H°_{acid}(A_0)$ value. Then, the kinetic method (for gas-phase acidity determination) can be rationalized by Equations (1) and (2) with the introduction of the GA^{app} term (apparent gas-phase acidity) by analogy with the GB^{app} (apparent gas-phase basicity) introduced by Wesdemiotis [8]. It should be stressed that the effective temperature (T_{eff}) is a fictional Maxwell-Boltzmann distribution representation of the internal energy of the activated dissociating dimeric ion (within the fragmentation time-window of the analyzer) and is not really equivalent to a thermodynamic temperature [9–11].

$$ln\frac{I[A_i - H]^-}{I[A_0 - H]^-} \approx ln\frac{k_i}{k_0} \approx -\frac{\Delta H°_{acid}(A_i)}{RT_{eff}} + \frac{GA^{app}(A_0)}{RT_{eff}} \quad (1)$$

$$GA^{app}(A_0) = \Delta H°_{acid}(A_0) - T_{eff}\Delta\Delta S°_{acid}(A_0, A_i) \quad (2)$$

Armentrout later established improved mathematical treatments of the extended method, the alternative and statistical methods, which avoid correlation in the quantities derived from Equation (1) [12]. With the alternative method, $GA^{app}(A_0)$ and T_{eff} are determined from the x-intercept and slope of the first kinetic method plot: $ln(k_i/k_0)$ versus $\Delta H°_{acid}(A_i)$. Then, a second plot, $GA^{app}(A_0)$ versus T_{eff}, allows the determination of $\Delta H°_{acid}(A_0)$ and $\Delta\Delta S°_{acid}(A_0, A_i)$, which correspond to the y-intercept and the slope of the line, respectively, according to Equation (2). It should be noted that the $ln(k_i/k_0)$ versus $\Delta H°_{acid}$ curves obtained at various activation conditions should ideally present a common crossing point called the "isothermal point" [13] or more accurately "isoequilibrium point" [7] and its abscissa corresponds to $\Delta H_{acid}(A_0)$. It should be noted that $\Delta\Delta S°(A_0, A_i)$ is negligible when the isoequilibrium point is in proximity to the x-axis. Importantly, the $\Delta\Delta S°(A_0, A_i)$ values are not exactly constant for dissociations of each noncovalent dimer, which means that a true isoequilibrium point cannot actually exist. Generally, if the distribution in $\Delta\Delta S°(A_0, A_i)$ values is not too large, uncertainties in the $\Delta H_{acid}(A_0)$ value obtained are minimized because these effects are averaged by the linearization in the $GA^{app}(A_0)$ versus T_{eff} curves.

The statistical method [12] more rigorously removes cross-correlation in the second kinetic method plots by introducing $\Delta H°_{acid}(A_i)_{avg}$, the average gas-phase acidity of all references used. Now the plots $ln(k_i/k_0)$ versus $[\Delta H°_{acid}(A_i)\text{-}\Delta H°_{acid}(A_i)_{avg}]$ obtained for each collision energy yield straight lines according to Equation (3). From the slope, $-1/RT_{eff}$, and y-intercept, $[GA^{app}(A_0)\text{-}\Delta H°_{acid}(A_i)_{avg}]/RT_{eff}$, the $[GA^{app}(A_0)\text{-}\Delta H°_{acid}(A_i)_{avg}]/RT_{eff}$ versus $(1/RT_{eff})$ relation ideally yields a linear dependence. Both the $\Delta H°_{acid}(A_0)$ and $\Delta\Delta S°(A_0, A_i)$ values are consequently easily deduced because the slope and the y-intercept represent $[\Delta H°_{acid}(A_0)\text{-}\Delta H°_{acid}(A_i)_{avg}]$ and $-\Delta\Delta S°(A_0, A_i)/R$, respectively, as shown by Equation (4).

$$ln\frac{k_i}{k_0} = \frac{GA^{app}(A_0) - \Delta H°_{acid}(A_i)_{avg}}{RT_{eff}} - \frac{\Delta H°_{acid}(A_i) - \Delta H°_{acid}(A_i)_{avg}}{RT_{eff}} \quad (3)$$

$$\frac{GA^{app}(A_0) - \Delta H°_{acid}(A_i)_{avg}}{RT_{eff}} = \frac{\Delta H°_{acid}(A_0) - \Delta H°_{acid}(A_i)_{avg}}{RT_{eff}} \quad (4)$$

$$- \frac{\Delta\Delta S°(A_0, A_i)}{R}$$

Again, this approach assumes that $\Delta\Delta S°(A_0, A_i)$ values are constant, when in fact, they cannot be.

Although Cooks' kinetic method is widely used because of its apparent simplicity and ease of use, it has also been subject to criticism by its abusive use. The main reason for its large success is that the kinetic method can be applied using almost all commercial tandem mass spectrometers. In the literature, several nonlinear effects have been observed upon the use of the kinetic method [6, 11, 14, 15]. Indeed, Drahos and Vékey have shown that the first kinetic method plot $[ln(k_i/k_0)$ versus $\Delta H°_{acid}(A_i)]$ is not strictly linear [14]. Such nonlinearity necessarily induces a reduction in the accuracy of the basicity/acidity measurements as they are based on assumed linear regression analyses. This deviation appears to be particularly significant for small molecules presenting a large entropic effect and is reinforced at higher activation energies. Nonlinearities have been also observed in the second kinetic method plot of the alternative approach, $GA^{app}(A_0)$ versus T_{eff} [11]. These non-linear effects have been interpreted as resulting from artifacts occurring at high or low energy conditions [11] or resulting from the existence of various isomeric forms within the dimer [15]. Significantly, nonlinear effects probably exist in many other studies but are masked by the cross-correlation inherent in the second kinetic plot of the conventional extended method, as demonstrated below.

In this paper, we are interested in more thoroughly exploring nonlinear effects occurring in the second plot $[GA^{app}(A_0)$ versus $T_{eff}]$ used for the alternative approach to the *extended* kinetic method, and even more apparent in the

second plot of the statistical approach. Two examples are discussed. The first example concerns an experimental determination of $\Delta H°_{acid}$ of substituted phenols, compounds that have been already widely investigated to determine their thermochemical properties (basicity [16], acidity [17, 18], cation and electron affinities). The results of this study compelled us to examine the second example, which concerns proton affinity determination of theoretical model molecules for which the thermochemical properties are known exactly. It is shown that even in this ideal case, the approximations required to apply the extended kinetic method still result in nonlinear plots of the data.

Materials and Methods

Chemicals

All compounds were purchased from Sigma-Aldrich (Saint-Quentin Fallavier, France). Substituted phenols and references (Table 1) were diluted in methanol at a concentration of 70 pmol μL^{-1} for experiments carried out on the triple quadrupole and 30 pmol μL^{-1} with the other mass spectrometers. In order to improve ionization efficiency, 0.1 % (vol/vol) of triethylamine was added to the solution.

Mass Spectrometry

All experiments were performed using electrospray ionization operated under the negative ion mode. Desolvation conditions were relatively soft to preserve the deprotonated noncovalent heterodimers. The solutions were infused into the ESI source using a syringe pump (flow rate of 160–400 $\mu L\ h^{-1}$). Three different mass spectrometers have been used: (1) a triple quadrupole (QQQ) instrument (Quattro I; Micromass, Manchester, United Kingdom), (2) a quadrupole ion trap (Esquire 3000; Bruker Daltonics, Bremen, Germany), and (3) a hybrid Qq-TOF (QSTAR Pulsar Hybrid QqTOF; Applied Biosystems, Courtaboeuf, France). The competitive dissociations of the studied noncovalent heterodimers were carried out under CID conditions with a collision voltage range of 0.2– 0.8 V_{p-p} for the ion trap mass spectrometer, 0–26 V for the QQQ instrument,

and 0–13 V for the Qq-TOF hybrid mass spectrometer. Helium was used as collision gas for the ion trap mass spectrometer ($P_{collision\ cell} = 10^{-3}$ mbar), whereas argon was used with the QQQ instrument ($P_{collision\ cell} = 5 \times 10^{-5}$ mbar), and nitrogen for the Qq-TOF hybrid mass spectrometer (arbitrary value of 1 for pressure in collision cell). (For the QQQ instrument, the pressure was kept as low as possible in order to be close to single collision conditions while still obtaining sufficiently abundant product ions at lower collision energies. The estimated average number of collisions is close to unity.) Weighted orthogonal distance regression (ODR) using the ODRPACK suite of programs [19] was used for PA and $\Delta\Delta S°$ calculations as implemented in the ODRFIT program described elsewhere [7]. Uncertainties in these values are quoted as 95 % confidence intervals.

Theoretical Calculations

Density functional theory (DFT) calculations were performed using Gaussian 03 software [20]. Optimized geometries of the neutrals and anions were conducted at the B3LYP/aug-cc-pVDZ level of theory followed by single point calculations using the aug-cc-pVTZ basis set and B3LYP, B3P86, and MP2 (full) levels of theory. Final values are corrected for zero point energy and thermal effects using a rigid rotor/harmonic oscillator approximation to yield $\Delta H°_{298}$ values.

Results

Experimental Gas-Phase Acidity Results of Substituted Phenols

Each deprotonated heterodimer, comprising an analyte (halogenated phenol) and a reference (carboxylic acid), was prepared with an electrospray ionization source. Table 1 lists the various species considered and their $\Delta H°_{acid}$ values taken from the literature. Our experimental source conditions were tuned in order to avoid the dissociation of noncovalent heterodimers in the limit of their lifetimes. Figure S1a in the Supplemental Material presents the mass spectrum obtained for an *ortho*-fluoro phenol/valeric acid mixture with the QQQ instrument. The proton-bounded heterodimer

Table 1. Molecular Weights and $\Delta H°_{acid}$ of the Phenols (R-C$_6$H$_4$-OH) and Carboxylic Acid (R′-COOH) References

Substituted phenols	R	M_w (u)	$\Delta H°_{acid}$ [a] $kJmol^{-1}$	Carboxylic acids	R′	M_w (u)	$\Delta H°_{acid}$ [b] $kJmol^{-1}$
o-F phenol	o-F	112	1447±12	Ethoxyacetic acid [49]	C$_3$H$_7$O	104	1431±9
p-F phenol	p-F	112	1455±10	4-Pentenoic acid [50]	C$_4$H$_7$	100	1441±12
o-Cl phenol	o-Cl	128	1437±10	*trans*-2-Pentenoic acid [50]	C$_4$H$_7$	100	1444±12
m-Cl phenol	m-Cl	128	1433±21	Cyclopentylacetic acid [49]	C$_6$H$_{11}$	128	1446±9
p-Cl phenol	p-Cl	128	1438±10	Valeric acid [49]	C$_4$H$_9$	102	1449±9
				Butyric acid [49]	C$_3$H$_7$	88	1450±9
				Propionic acid [49]	C$_2$H$_5$	74	1454±9
				Acetic acid [18]	CH$_3$	60	1459±9

[a]From NIST Webbook [45] with Original Data Using Ion/Molecule Reaction Equilibria [27].
[b]From NIST Webbook [45] with Original Data Using Ion/Molecule Reaction Equilibria [18, 49] and Kinetic Method [50] Approaches.

$[A_0+A_i-H]^-$ (m/z 213) is produced in good yield reflecting its gas-phase stability under the soft desolvation conditions used. The distribution of homo- and heterodimeric m/z 203, 213, 223 ions is not statistical, a feature that is relevant to differences in their relative stabilities [21]. Low-energy collision-induced dissociations (CID) of the $[A_0+A_i-H]^-$ heterodimers yielded the two corresponding competitive deprotonated molecules $[A_0-H]^-$ (m/z 111) and $[A_i-H]^-$ (m/z 101) (Supplementary Figure S1b). It should be stressed that consecutive decompositions were observed in certain cases. Strikingly, several carboxylic acid references yielded significant secondary generation of product ions produced by loss of carbon dioxide from 4-pentenoic and *trans*-2-pentenoic acid anions and induced by losing ethene molecule from ethoxyacetic acid anion. These ions were included in the data analysis by simply adding them to the primary product ion signal.

These experiments have been repeated under various activation conditions for all substituted phenols. In this paper, we present data obtained primarily by using laboratory frame collision energies from 2 to 22 eV in the collision cell of the QQQ mass spectrometer, a range for which nonlinear effects could be observed in some systems. The use of laboratory frame energies is primarily one of convenience because the same energy is required for all systems shown in a kinetic plot, which is of course why most presentations in the literature also follow this protocol. It is probably more appropriate to examine the data on the same center-of-mass frame scale, as these are the energies truly available for the reaction being considered and differences among references can occur especially if they differ appreciably in mass. However, in order to have the same energy for all systems, this requires interpolation of the data, which also introduces some smoothing. For the systems examined here, we have performed this operation and found that it does *not* significantly change the character of the results, although a slight improvement in the range of linearity was obtained (data not reported). This latter result suggests that the additional work associated with the energy scale conversion may be worthwhile, but we proceed using the more convenient and conventional laboratory scale energies.

Figure 1a and b present the plot of $\ln(k_i/k_0)$ versus $\Delta H^\circ_{acid}(A_i)$ for *ortho*-fluorophenol and *para*-fluorophenol, respectively. In the following discussions, only these two isomers are described in detail but all data are reported in Table 2. For the *ortho*-fluoro derivative (Figure 1a), the lines for all activation energies cross at one point: the isoequilibrium point; however, there is no single isoequilibrium point for the *para*-isomer (Figure 1b). It should be noted that only collision energies at or below 22 eV are reported in these curves and used for the acidity determinations. Indeed, above this energy, the effective temperature (T_{eff}) value does not rise smoothly with the collision energy, as seen in Figure 1c and d.

The alternative and statistical treatments [12] were used to determine the $\Delta H^\circ_{acid}(A_0)$ values (Figure 2). According to the alternative approach, the $GA^{app}(A_0)$ versus T_{eff} plot for *ortho*-fluorophenol (Figure 2a) is characterized by a straight line that evolves in the T_{eff} range from 450 to 1100 K. The intercept and slope of this line provides $\Delta H^\circ_{acid}(A_0)=$ 1446 kJmol^{-1} and $\Delta\Delta S^\circ=-9$ JmolK^{-1}, respectively. In contrast, two slopes are observed for the *para*-fluorophenol over the same T_{eff} range. The first line was in the 500–850 K range and the second between 850 and 1100 K (Figure 2c), corresponding to acidity values of 1447 and 1454 kJmol^{-1}, respectively. The gas-phase acidity of this compound was also investigated by using the *statistical* approach, known to remove errors in the second plot of $[GA^{app}(A_0)-\Delta H^\circ_{acid}(A_i)_{avg}]/RT_{eff}$ versus $(1/RT_{eff})$ [12]. In the case of *ortho*-fluorophenol (Figure 2b), the statistical approach again leads to a $[GA^{app}(A_0)-\Delta H^\circ_{acid}(A_i)_{avg}]/RT_{eff}$ versus $(1/RT_{eff})$ plot characterized by a single straight line. For *para*-fluoro phenol, the statistical approach also yields two slopes (Figure 2d), but the slope difference between the two lines is reinforced. (In this case, note that the two slopes have different signs, indicating that the relative acidity is lower than $\Delta H^\circ_{acid}(A_i)_{avg}=1451.6$ kJ/mol at low energies and higher at high energies.) Both the alternative and statistical approaches give the same ΔH°_{acid} values (as expected) within 1 kJmol^{-1}, well within the estimated experimental errors (Table 2). It can also be noted that an ODR analysis provides nearly identical results when applied over the same energy ranges for both *ortho*- and *para*-fluorophenol. These results are in agreement with the unique isoequilibrium point observed in Figure 1a for *ortho*-fluorophenol, whereas careful scrutiny of Figure 1b shows two (or more) isoequilibrium points for *para*-fluoro phenol.

If the original extended method [5] is applied to these data, the $GA^{app}(A_0)/RT_{eff}$ versus $1/RT_{eff}$ plot appears to be a straight line with a regression coefficient close to $R^2=1.0000$ for both fluoro phenols. From this approach, one experimental acidity value is obtained, 1446±5 and 1449±5 kJ mol^{-1}, for *ortho*- and *para*-fluorophenols, respectively. The very good regression coefficient obtained by this method is a result of the self-correlation of the data [12]. Hence, the original extended method does not allow the observation of these two slopes for *para*-fluorophenol, a feature that probably explains why such behavior has not often been described previously. However, this phenomenon has been observed previously, e.g., two isoequilibrium points can be distinguished on the $\ln(k_i/k_0)$ versus $\Delta H^\circ_{acid}(A_i)$ plots for the acidity measurements of urea in the literature [22], corresponding to two acidities values: 1514 and 1518 kJ mol^{-1}. In this case, the use of the original extended method prevented the authors from observing two lines in the second kinetic method plot. Whereas this difference of 4 kJmol^{-1} for urea could easily be a result of experimental uncertainties, in the present case, the change in the gas-phase acidity values is more significant for *para*-fluoro phenol at 7 kJmol^{-1}. This behavior is not unique as shown in Table 2, where two experimental acidities are characterized for *para*-fluoro as well as *ortho*, *meta*, and *para*-chloro phenols, with
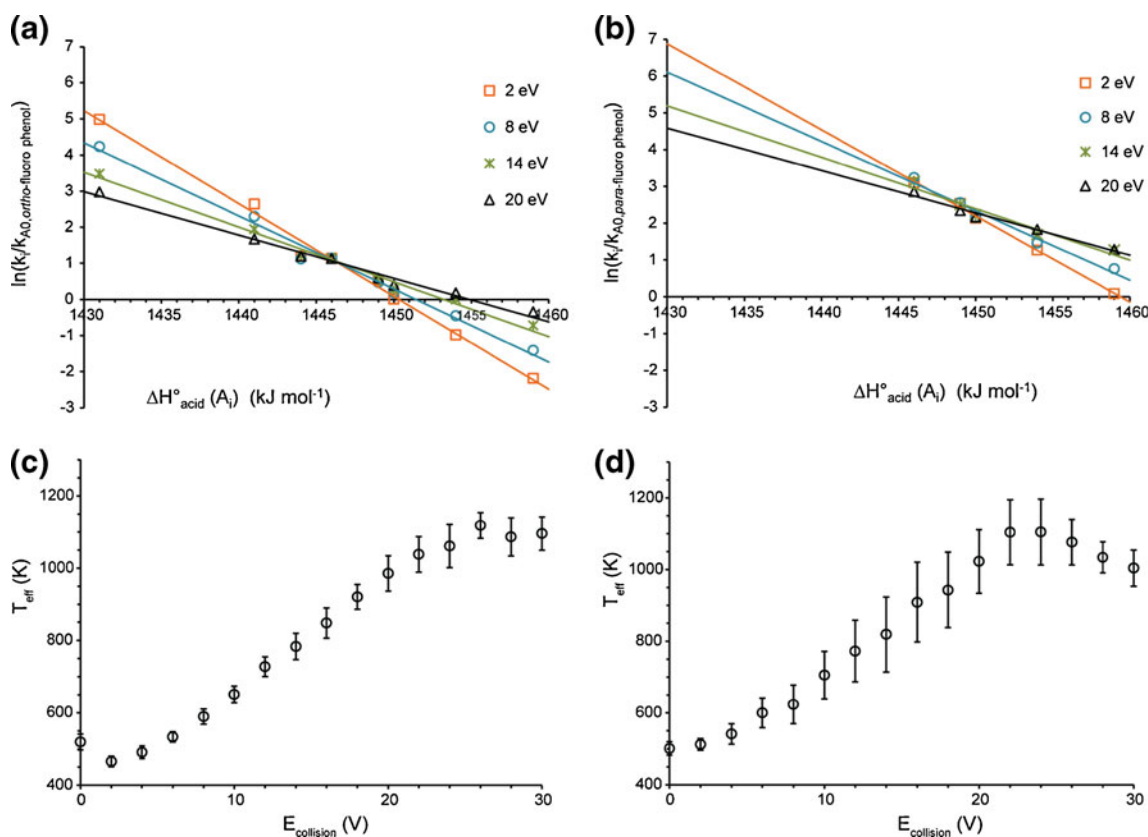
Figure 1. Plots of $\ln(k_i/k_0)$ versus $\Delta H°_{acid}(A_i)$ obtained from experiments performed with the triple quadrupole for **(a)** *ortho*-fluorophenol and **(b)** *para*-fluorophenol. Plots of T_{eff} versus $E_{collision}$ for **(c)** *ortho*-fluorophenol and **(d)** *para*-fluorophenol

differences of 4–9 kJmol^{-1}. Only *ortho*-fluoro phenol presents a single acidity value. (Interestingly, even though the *ortho*-fluoro phenol results appear linear in all data formats, if the low and high data are independently analyzed, they also yield different $\Delta H°_{acid}$ values: 1444.6±2.4 kJmol^{-1} and $\Delta\Delta S° = -11.7\pm3.9$ J mol^{-1}K^{-1} for 2 – 14 eV, and $\Delta H°_{acid} = 1451.1\pm8.7$ kJmol^{-1} and $\Delta\Delta S° = -3.7\pm9.4$ Jmol^{-1}K^{-1} for 14–22 eV, with a difference in acidities of 6.5 kJmol^{-1} that is comparable to the other cases.) Results obtained from the alternative, statistical, and ODR methods are essentially the same when analyzed over the same energy ranges, with differences less than 1 kJmol^{-1} (as expected).

In the case of *para*-fluorophenol, the $\Delta H°_{acid}$ value obtained at lower effective temperatures is smaller than that recorded at higher effective temperatures. As the origin of the two experimental acidity values is unclear, we wondered if this phenomenon is inherent to assumptions required by the extended kinetic method. First, good linear plots were obtained for the $\ln(k_i/k_0)$ versus $\Delta H°_{acid}(A_i)$ curves, Figure 1b, suggesting that T_{eff} is similar for each dimer system examined. Moreover, the $\Delta\Delta S°_{acid}(A_0, A_i)$ differences are not too large (~20 Jmol^{-1}K^{-1} for *para*-fluoro phenol and smaller for all other complexes) such that systematic errors in the determination of thermochemical parameters are not expected [6, 7]. The A_i compounds (i.e., aliphatic and alicyclic carboxylic acids) were chosen as

references because they are monofuctionnal and similar between themselves. Therefore it is expected that the entropy change differences ($\Delta\Delta S°_{acid}$) between the substituted phenols and the references are approximately constant (isoentropic conditions). However, as discussed by Ervin and Armentrout [7], even with such references, the constant entropy exchange assumption is never exactly true.

Similar experiments have also been carried out for the *para*-fluorophenol system using a quadrupole ion trap and a hybrid quadrupole-time-of-flight instrument (Qq-TOF) (Figure 3 and Supplementary Figure S2). Note that these data do not include the cyclopentylacetic acid reference because it cannot be used with the ion trap or Qq-TOF instrument as their dynamic range is not high enough, i.e., only deprotonated cyclopentylacetic acid is observed in the decomposition of the $[C_6H_{11}COO^-$ H^+ $^-OC_6H_4pF]$ dimer. This helps explain why the double slope in the QQQ data is not as pronounced in Figure 3 (although still clearly present) as in the comparable plots of Figure 2c and d. Figure 3 shows that the ion trap yields a low T_{eff}, around 300 K, that does not rise significantly with the resonant collision energy, as generally observed with this instrument [23–25]. The Qq-TOF is equipped with the LINAC^{TM} collision cell, that allows trapping of the ions in order to increase the duty cycle [26]. Interestingly, in this condition, T_{eff} is between that of the quadrupole ion trap and the triple quadrupole. The

Table 2. Experimental Values of ΔH°_{acid} and $\Delta\Delta S^{\circ}(A_0, A_1)$ obtained using the Alternative and Statistical Methods and A Comparison with Both Theoretical and Literature Values of ΔH°_{acid}

Substituted phenols	E_{coll} (eV)	T_{eff} (K)	Experiment[a]						Theory	Literature
			Alternative method		Statistical method		ODR[b]			
			ΔH°_{acid} (kJmol⁻¹)	$\Delta\Delta S^{\circ}(A_0, A_1)$ (Jmol⁻¹K⁻¹)	ΔH°_{acid} (kJmol⁻¹)	$\Delta\Delta S^{\circ}(A_0, A_1)$ (Jmol⁻¹K⁻¹)	ΔH°_{acid} (kJmol⁻¹)	$\Delta\Delta S^{\circ}(A_0, A_1)$ (Jmol⁻¹K⁻¹)	ΔH°_{acid}[c] (kJmol⁻¹)	ΔH°_{acid}[d] (kJmol⁻¹)
o-F phenol	2–22	450–1100	1446±5	−9±10	1447±5	−9±10	1446.2±1.3	−8.9±1.7	1444, 1450, 1442	1447±12
p-F phenol	2–14	500–850	1447±5	−23±10	1447±5	−23±10	1449.8±1.2	−19.5±1.5	1446, 1452, 1444	1455±10
	14–22	850–1100	1454±5	−15±10	1454±5	−15±10				
o-Cl phenol	2–8	400–600	1444±5	10±10	1444±5	9±10	1437.6±1.9	−2.9±2.4	1435, 1441, 1435	1437±10
	8–26	600–1150	1435±5	−5±10	1436±5	−5±10				
m-Cl phenol	4–10	500–700	1434±5	0±10	1435±5	1±10	1428.0±3.4	−9.8±3.7	1423, 1429, 1423	1433±21
	10–26	700–1250	1426±5	−12±10	1427±5	−11±10				
p-Cl phenol	2–14	500–800	1438±5	−4±10	1437±5	−7±10	1434.5±3.2	−10.8±4.1	1429, 1435, 1429	1438±10
	14–20	800–1250	1433±5	−11±10	1433±5	−13±10[a]				

a The overall errors (including inherent errors of the kinetic method), of ion abundance measurements, and relative uncertainties in reference compound thermochemistry) are ±5 kJmol⁻¹ for ΔH°_{acid} and ±10 Jmol⁻¹K⁻¹ for $\Delta\Delta S^{\circ}[A_1{\rightarrow}A_0]$ [45]. These values do not include the absolute uncertainties of the reference thermochemistry.
b Orthogonal distance regression (ODR) results over the entire energy range. Uncertainties are 95 % CI and do not include the absolute uncertainties of the reference thermochemistry.
c Acidities values obtained using theoretical calculations at the R/aug-cc-pVTZ//B3LYP/aug-cc-pVDZ level of theory where R=B3LYP, B3P86, and MP2(full) including zero point and thermal corrections.
d Acidities values obtained from literature [27].

lowest T_{eff} value is very close to that obtained with the ion trap, but T_{eff} rises significantly with the increase of the collision energy (up to 410 K). Alternative and statistical analyses of the Qq-TOF data yield ΔH°_{acid}(A_0)=1451±5 kJ mol⁻¹, midway between the values obtained for the low and high T_{eff} ranges in the QQQ instrument. In the present case, the use of either statistical or alternative methods to analyze the ITMS, Qq-TOF, and low-energy QQQ data together yield a value for ΔH°_{acid}(pFC$_6$H$_4$OH) of 1447.9±0.3 kJmol⁻¹ (1447.3±0.3 kJmol⁻¹ for a weighted fit), in agreement with the value obtained for the lower collision energy range of the QQQ data, Table 2. Because of the more limited range of temperatures accessed by these alternative experimental results, they do not exhibit the nonlinearities evident in the QQQ data. In particular, the ion trap data alone have a very small T_{eff} range ($\Delta T_{eff}{\approx}7$ K here), such that accurate thermochemical data cannot be obtained using these data alone. Hence, similar studies were not pursued for systems other than *para*-fluorophenol.

Results from the Literature and from DFT Calculations

The ΔH°_{acid} values experimentally obtained for substituted phenols were compared with those obtained by DFT calculations and experimental values reported in the literature (Table 2). ΔH°_{acid} values from the literature presented here were measured by means of the equilibrium method. From the two major acidity reference scales, we choose those determined by McMahon and Kebarle, as this work includes most of the species studied in the present work [27]. In the case of *ortho*-fluorophenol, the experimental value obtained here is in very good agreement with that reported in the literature. For the *p*-F and *o*-Cl phenols, the literature values are in better agreement with the value corresponding to the higher T_{eff} range. In contrast, for *m*-Cl and *p*-Cl phenols, the literature values are in better agreement with the experimental line corresponding to the lower T_{eff} range. In all cases, values obtained at both low and high T_{eff} ranges agree with the literature values within experimental uncertainties.

To obtain additional clues to explain our experimental results, quantum chemical calculations were carried out highlighting the relative acidity associated with the M→ [M-H]⁻+H⁺ equation. Overall, experimental and theoretical 298 K acidity values present a fairly good correlation (Table 2), with mean absolute deviations of 7±4 kJmol⁻¹ for the B3LYP and MP2(full) approaches and 4±1 kJmol⁻¹ for the B3P86 calculations. The signed deviations show that the former approaches are systematically low by about 4 %, whereas the B3P86 predictions are evenly distributed about the experimental results. Notably, the quantum chemical calculations provide no obvious explanation for the existence of two slopes (or two acidities) in the experimental results. In particular, this phenomenon cannot be explained by the existence of several isomers as observed for other systems [28]. An implicit assumption of the kinetic method
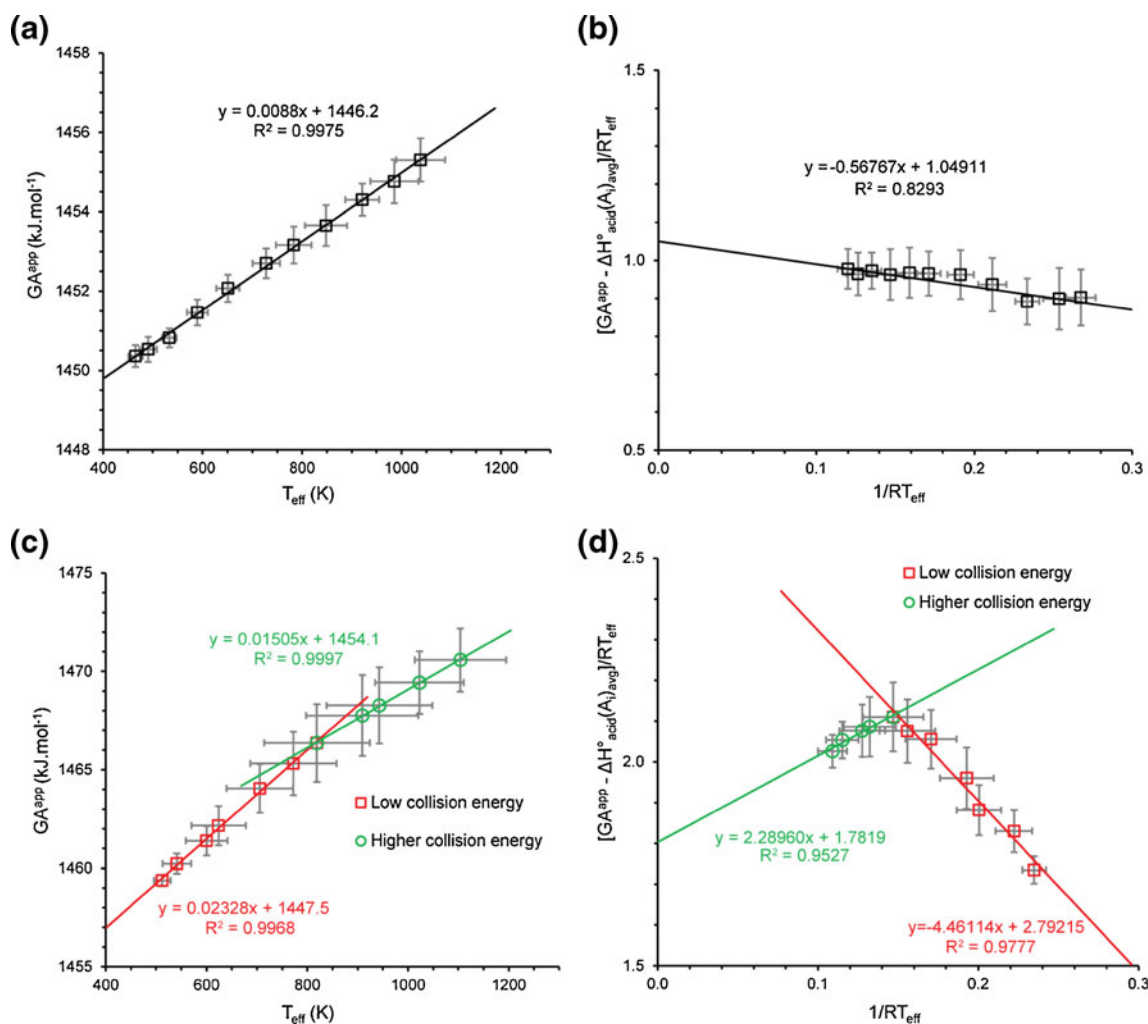
Figure 2. Alternative approach: Plots of GA^{app} versus T_{eff} for **(a)** *ortho*-fluorophenol and **(c)** *para*-fluoro phenol. Statistical approach: Plots of $[GA^{app} - \Delta H°_{acid}(A_i)_{avg}]/RT_{eff}$ versus $[1/RT_{eff}]$ for **(b)** *ortho*-fluorophenol and **(d)** *para*-fluorophenol. Data obtained using the triple quadrupole with low (2–14 eV) and high (14–22 eV) energies

is that the dissociating dimer has only one structure. Lorenz and Rizzo have shown that for dimers of multifunctional amino acids, this is not always the case and different isomers can be experimentally evidenced [28]. In the present work, all monomers are monofunctional, such that the existence of various isomers is unlikely. Although different conformers can be considered, they will not differ in their deprotonation sites. Complications associated with different conformers of deprotonated carboxylic acid dimers have been explored by Ervin and coworkers and were used to explain some inconsistencies in the acidity measurements [29]. This work also demonstrated that only the ground state Z conformers of the carboxylic acids (associated with having the hydroxyl group be oriented *cis* relative to the carbonyl) contribute appreciably to the dissociation, whereas the E conformers (trans hydroxyl orientation) are sufficiently high in energy (>20 kJmol^{-1}) that their contributions to the dissociation are negligible. Additional calculations performed here confirm that the E conformers of the other acids also lie 19–21 kJ/

mol above the Z conformers. These calculations also show that the lower energy Z conformers of the acids are the conformer involved in the ground state complexes with the phenols.

Double Slopes: Reality or Artifact?

In principle, the existence of the two slopes could be a result of different experimental issues occurring either at low or high activation conditions. At low collision energy, product ion abundances may be too low to measure accurately, in particular if the difference in branching ratio is large. It can be postulated that $\ln(k_i/k_0)$ should not be larger than 4, corresponding to the measurement of a relative intensity of 2 % for the less abundant fragment ion produced from the decomposition of the noncovalent dimer. This value could be adjusted depending on the dynamic range of the instrument used. At high collision energy, several effects may contribute to the anomalies. First, consecutive decom-
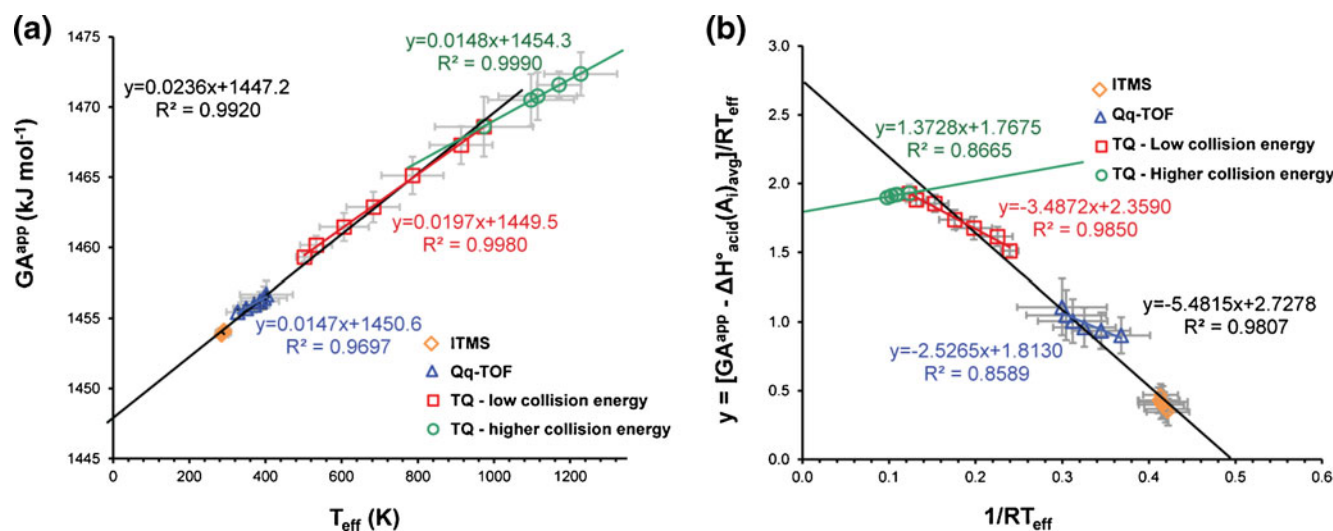
Figure 3. Kinetic method plots for *para*-fluorophenol obtained with ion trap (ITMS), Qq-TOF, and triple quadrupole (TQ). **(a)** Alternative approach and **(b)** statistical approach. The linear regression line in black includes all data points with the exception of the higher energy TQ points. Linear regression lines in blue, red, and green correspond to the Qq-TOF, low-energy TQ, and high-energy TQ data, respectively. Fitting parameters are provided in all cases. These curves have been plotted without the cyclopentylacetic acid

positions may take place; although this should be overcome by taking into account the intensity of the consecutive product ions by adding their abundance to that of the corresponding primary deprotonated monomer. This presumes that there are no collection efficiency differences in the primary and secondary product ions. Second, fragmentation efficiency may level off or be reduced at high activation energy. In Figure 1c and d, it can be observed that T_{eff} rises almost linearly with the collision voltage up to about 20 eV. After 20 eV, the effective temperature levels out or declines with increasing collision energy, whereas in theory, the T_{eff} values should continue to increase [10, 30]. A continued quasi-linear increase is not expected theoretically, because of angular momentum constraints associated with bimolecular collisions. This high energy behavior alone cannot explain the double slopes observed in the second kinetic method plots of Figure 2, which avoid the high-energy ranges associated with this behavior. Third, m/z discrimination may occur at high collision energy that can lead to errors in the determination of the k_i/k_0 ratio. This consideration is particularly important in the case of quadrupole ion trap instruments because of the low-mass cut-off corresponding to about 20 %–33 % of the precursor ion m/z [31]. Other discrimination effects may be related to ion scattering losses in QQQ and Qq-TOF instruments [32], where product ions with relatively high kinetic energy are not collected and detected. Such behavior may be involved in the evolution of T_{eff} with the collision energy in Figure 1c and d. However, because this effect is controlled by the relative masses of the dimer fragments, it cannot explain the difference in behavior between the *ortho*-fluoro and *para*-fluoro phenol systems.

The number of references and the available acidity range has a great influence on the determination of the slope of the ln

(k_i/k_0) versus $\Delta H°_{acid}$ plot. Our *ortho*-fluorophenol kinetic plot was done using 8 references with about 30 kJmol^{-1} of acidity range, Figure 1a. By contrast, the *para*-fluorophenol data, Figure 1b, uses only five references because some references such as ethoxyacetic acid have gas-phase acidity and entropy differences that are too large. In order to compare these results in a more rigorous way, three of the references can be removed from *ortho*-fluorophenol plot, but the curves and *isoequilibrium* crossing point obtained remain largely unchanged.

Modeling of the Two Competitive Channels for the Different Systems Studied

Instead of analyzing the QQQ data using the kinetic method approach, the kinetic energy dependence of the dissociation yields can be modeled using the statistical methods developed for analysis of energy-resolved collision-induced dissociation [33–36], which includes Rice-Ramsperger-Kassel-Marcus (RRKM) statistical rate theory [37, 38] to evaluate kinetic and competitive shifts. The *CRUNCH* Fortran program [36] was used to model the competitive threshold collision-induced dissociation (TCID) of the *para*-fluorophenol/carboxylic acid deprotonated heterodimers. Using *CRUNCH*, fits for the normalized A_1 and A_0 experimental ion peak intensities (logarithmic scale) plotted as a function of the center-of-mass collision energy were analyzed and reproduced (see Supplementary Figure S3).

For these simulations, the ion beam kinetic energy distribution was estimated by analysis of experimental retarding potentials. A relatively large kinetic energy distribution (FWHM) equal to 1.7 eV and a shift in the zero of 0.7 eV towards lower energy values compared to the

nominal applied energy were observed. This broadening probably results from the first quadrupole because ions are not extracted only from the center. The offset in energy is also typical and can be the result of many factors. The dominant factor is probably a field in the source region where the zero voltage for the ions is established, but additional factors could include contact potential differences between the source and the region where the ions are measured and aberrations in the focusing.

For this modeling, the total internal energy of the energized complex E^* is given by its initial thermal energy distribution [39, 40] plus the energy ε acquired from the collision with argon gas. This process is modeled with the empirical energy-transfer distribution function Equation (5). E is the relative collision energy in the center-of-mass reference frame, σ_0 is an energy-independent scaling factor related to the total collision cross section, and N is an adjustable parameter that describes the efficiency of translational to internal energy transfer [29, 41].

$$P_e(\varepsilon, E) = \sigma_0 N \frac{(E - \varepsilon)^{N-1}}{E} \quad (5)$$

The probability for dissociation, $P_D(\varepsilon)$, is given by $1 - \exp[-k_{total}(E^*)\tau]$, where $k_{total}(E^*)$ is the total unimolecular rate constant of dissociation as given by RRKM theory, the reaction occurs only when $E^* \geq E_0$, and τ is the time available for dissociation (here 10^{-4} s). Branching into the two pathways is controlled by $k_j(E^*) / k_{total}(E^*)$ where $k_{total}(E^*) = k_1(E^*) + k_2(E^*)$ for channels $j=1$ and 2. The transition states for product formation are treated as orbiting TSs (loose, i.e., located at the centrifugal barrier). Overall the model for the experimental cross sections of a particular channel j is given by Equation (6),

$$\sigma_j(E) = S_0(j) \int \left[k_j(E^*)/k_{total}(E^*)\right] P_D(\varepsilon) P_e(\varepsilon, E) d\varepsilon \quad (6)$$

where $S_0(j)$ is a scaling factor for channel j. This equation can be compared to the data after convoluting over the kinetic and internal energy distributions of the reactants.

The optimized critical energy values (E_0) and the differences of critical energy values (ΔE_0) for the two competitive channels are reported in Table 3. Thermal enthalpy corrections from 0 to 298 K (calculated with the rigid-rotor/harmonic oscillator approximation) are included to obtain corresponding $\Delta\Delta H°_{298}$ values. For the [CH$_3$COO$^-$ H$^+$ $^-$OC$_6$H$_4p$F] dimer, two different variations of the loose transition states were used (Table 3 and Supplementary Figure S3). First, independent adjustable scaling factors (model a) are employed to improve the fit to the experimental data and allow fitting over a wider collision energy range. Optimal values of $S_0(1)=1$ and $S_0(2)=0.33$ were obtained from simulations

Table 3. Analysis of the Dissociation of [R'COO$^-$ H$^+$ $^-$OC$_6$H$_4p$F] Dimers with TCID Modeling[a]

R'	σ_0	N	$E_0(1)$ eV	$E_0(2)$ eV	ΔE_0 eV	$\Delta\Delta H^0_{298}$ kJmol^{-1}	$\Delta\Delta S$ Jmol^{-1}K^{-1}	$S_0(2)$	Energy Range (eV)
CH$_3$ [b]	0.48 (0.06)	1.2 (0.1)	1.10 (0.16)	1.07 (0.15)	-0.034 (0.008)	-3.7 (0.8)	-14 (1)	0.33 (0.05)	0.07-3.7
CH$_3$ [c]	0.53 (0.06)	1.1 (0.1)	1.15 (0.16)	1.10 (0.15)	-0.043 (0.013)	-4.5 (1.3)	-12 (1)	0.07 (0.02)	0.07-3.7
C$_2$H$_5$ [b]	0.55 (0.07)	1.2 (0.1)	1.06 (0.15)	1.05 (0.14)	-0.016 (0.005)	-1.9 (0.5)	-5 (1)	0.14 (0.01)	0.07-3.8
C$_3$H$_7$ [b]	0.71 (0.09)	1.0 (0.1)	1.20 (0.12)	1.20 (0.12)	0.001 (0.002)	-0.1 (0.2)	-4 (1)	0.16 (0.01)	0.06-3.9
C$_4$H$_9$ [b]	0.78 (0.10)	1.0 (0.1)	1.22 (0.12)	1.24 (0.12)	0.020 (0.004)	1.7 (0.4)	1 (1)	0.12 (0.01)	0.06-3.4
C$_6$H$_{11}$ [b]	1.04 (0.12)	0.8 (0.1)	1.39 (0.12)	1.45 (0.13)	0.064 (0.007)	6.0 (0.7)	0 (1)	0.24 (0.01)	0.05-4.2

[a] Uncertainties in parentheses.
[b] Orbiting TS model with all vibrations and second channel having an independent adjustable scaling factor $S_0(2)$, model a.
[c] Orbiting TS model with hindered rotors (CH$_3$COOH, σ=3, and HOC$_6$H$_4p$F, σ=2), a free rotor (CH$_3$COO$^-$, σ=6), and second channel having an independent adjustable scaling factor $S_0(2)$, model b.

of the two competitive decomposition channels. Such scaling factors suggest that at least one methyl rotor gets locked down by interaction with another part of the molecule in the heterodimer reactant. Second, the methyl rotor of CH_3COOH and phenyl rotor of HOC_6H_4pF are explicitly treated as hindered rotors rather than as vibrations and the methyl rotor of CH_3COO^- is treated as a free rotor (see Supplementary Figure S3 and Supplementary Table S1), which leads to an optimized scaling factor of $S_0(2)=0.07$ (model b).

From Table 3, one can notice that only small differences in the ΔE_0 values are measured depending on the model used (-0.03_4 and -0.04_3 eV). These differences are reduced slightly once the thermal enthalpy corrections to convert the thresholds to $\Delta\Delta H^0_{298}$ values are applied (-3.7 and -4.5 kJmol^{-1}) because the hindered rotors have different heat capacities than when treated as vibrations. Because of these small differences, the alternate approaches involving hindered and free rotations were not considered for any but the acetic acid dimer. The utility of using the same approach can be partially assessed by noting that the $\Delta\Delta H^0_{298}$ range between the two extreme references (acetic acid and cyclopentylacetic acid, -13 kJmol^{-1}, Table 1, with a relative uncertainty probably near 4–6 kJmol^{-1}) is close to that obtained from model a on both compounds, -9.7±1.1 kJmol^{-1}, Table 3.

Although not the major point of the present work, it is worth noting that the results of Table 3 can be used to derive a value for the acidity of *para*-fluoro phenol. If the 298 K acidities of the five references from Table 1 are combined with the $\Delta\Delta H°_{298}$ values, we obtain five values for $\Delta H°_{298,acid}$ (*para*-fluoro phenol) ranging from 1450 to 1455 kJmol^{-1}. The simple average of these five values is 1452.0±4.2 kJmol^{-1}, which does not include the uncertainties in the reference values (either relative or absolute), and their weighted average is 1450.6±0.9 kJmol^{-1} (uncertainties are two standard deviations). These determinations agree nicely with the literature value of 1455±10 kJmol^{-1}, as well as with the kinetic method approaches explored here, although it is interesting that the weighted average lies midway between the values obtained from the low and high T_{eff} ranges, Table 2. Notably, the weighted average agrees very well with the ODR result, within the 1 kJmol^{-1} uncertainty.

Modeling of the A_1 over A_0 Ratios for the Different Studied Dimers

Figure 4 shows the experimental ratios of A_i over A_0 ion peak intensities (logarithmic scale) as a function of the center-of-mass energy corresponding to collision voltages taken every 2 volts from 2 to 30 V in the laboratory frame for the five studied deprotonated dimers involving *para*-fluoro phenol. Calculated ratios obtained from the statistical modeling with Equation 6 and the parameters of Table 3 are also shown using full lines. For most of the dimers, the models reproduce the data relatively well through most of this energy range, whereas there are larger deviations,
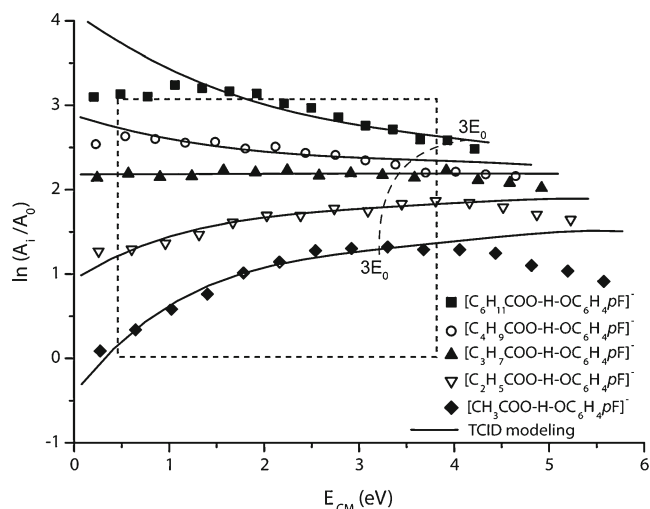

Figure 4. $\ln(A_i/A_0)$ versus E_{CM} for the different studied dimers [R-COO$^-$ H$^+$ $^-$OC$_6$H$_4$pF]. Points are experimental results and lines are obtained by TCID modeling. The rectangle indicated by the dashed line corresponds to the energy range and product ratios presenting good agreement between experimental and theoretical data. The $3E_0$ dashed line is approximately equal to three times the calculated critical energy

especially at higher energies. The range of data that seems most reproducible is highlighted by the dashed rectangle in Figure 4. The deviations between experiment and TCID modeling are observed for collision energy values above about 3 E_0 or E_{lab}=20 eV) and also at the lowest internal energies. Similar deviations have also been observed using more sophisticated instrumentation. For instance, guided ion beam studies of the [CH$_3$COO$^-$ H$^+$ $^-$OC$_6$H$_5$]$^-$ dimer, where the threshold is 0.98±0.30 eV, deviate from the TCID model for energy values lower than 0.7 eV and higher than 2.5 eV in the center-of-mass frame [42].

If the TCID model data shown in Figure 4 are plotted according to the kinetic method approaches over the range used in the analyses above, (i.e., 2–22 eV) the results in Figure 5a and b are obtained, where they are compared with the original data (reproduced from Figure 2c and d). As noted above, nonlinear deviations are observed in the second kinetic method plots when using the experimental data (e.g., $GA^{app}(A_0)$ versus T_{eff} (alternative method) and [$GA^{app}(A_0)$-$\Delta H_{avg}(A_i)$]/RT_{eff} versus $1/RT_{eff}$ (statistical method). Such nonlinear deviations are *not* observed from the corresponding plots that use the TCID model data (fitted curves of Figure 4). In part, this is because the TCID modeling explicitly evaluates variations in the entropy terms from system to system. Notably, the $\Delta H°_{acid}$ value obtained from the TCID model, 1451±5 kJmol^{-1}, matches that obtained from the ODR analysis of the original data over the same range of energies, Table 2. Given this conclusion, it is not surprising that when the kinetic plots are reconstructed considering only the area presenting good agreement

between experiment and TCID simulations (removal of the cyclopentylacetic acid reference data and restriction to a collision voltage range from 4 – 18 V in the laboratory), the nonlinear effects largely disappear for both alternative and statistical approaches (Figure 5c and d). Under these new conditions, one can notice that experimental data and calculated curves are nearly superimposable. It should be noted that removing only the cyclopentylacetic acid (keeping the full energy range) still yields a double slope as shown in Figure 3, although it is significantly attenuated. On the other hand, keeping the cyclopentylacetic acid reference but restricting the energy range between 2 and 18 V maintains a strong double slope (in practice, corresponding to the removal of the two highest energy points in Figure 5a and b). This shows that both the energy range and the references used can influence the nonlinear effects. This can be seen in Figure 4, where the "good" data points correspond to those within the dashed rectangle, as determined by agreement between the data and the ideal trends. Importantly, if the ODR model is used, the same ΔH°_{acid} values are obtained (deviations ≤0.6 kJmol^{-1}) for both 2–22 and 4–18 eV energy ranges with or without the

cyclopentylacetic acid reference. Furthermore, the ODR values lie within their 1.2 kJmol^{-1} uncertainty (Table 2) of the values obtained from analyses of the TCID model data in Figure 5. The same conclusions hold for the $\Delta\Delta S^{\circ}$ values derived in all cases.

For the dimers studied here, the possible coexistence of different isomers resulting from multiple hydrogen bonding interactions seems unrealistic and hence cannot explain the nonlinear effects observed. As noted above, dissociation to the higher energy E conformer of the carboxylic acid neutral has been demonstrated to contribute little to the observed dissociation [29]. Thus, these nonlinear effects are interpreted as resulting from artifacts occurring both at high and low energy conditions. Even in well-controlled guided ion beam mass spectrometry measurements, low-energy deviations can occur and are ordinarily the result of the uncertainties in the data, which are relatively large near threshold because the ion signals approach zero. At higher energies, collisions with rare gases can become more impulsive such that the statistical energy deposition assumed in the TCID modeling may no longer be appropriate. In the experiments performed here, divergences for low-energy
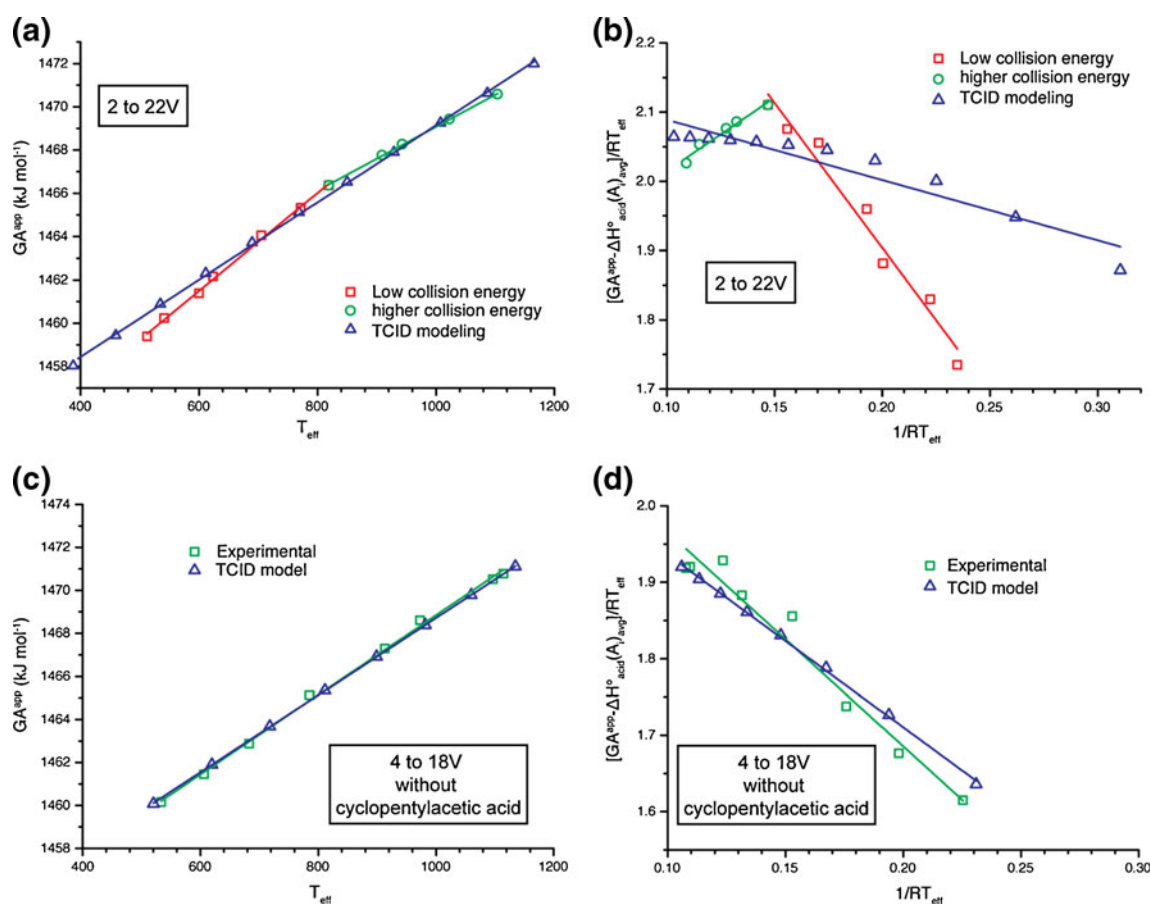

Figure 5. Experimental and TCID modeling of the second kinetic method plot for [R-COO$^-$ H$^+$ $^-$OC$_6$H$_4$pF] heterodimers; (a) and (c) alternative approach and (b) and (d) statistical approach. Parts (a) and (b) show curves obtained for collision voltages of 2–22 V. Parts (c) and (d) show curves obtained using a restricted voltage range of 4–18 V and removing the cyclopentylacetic acid reference

values can also occur as a result of DC offset voltages between the Q1 and Q3 analyzers and the h2 collision cell, which lead to higher energy collisions in these regions [41]. The lower-order fields in a hexapole (and especially a quadrupole collision region) introduce perturbations in the kinetic energy distributions of the reactant ions that are much larger than those of the octopole guide used in guided ion beam instruments. These phenomena are probably reinforced by the higher pressure conditions used here compared with those in well-controlled guided ion beam mass spectrometry measurements [43], in order to obtain adequate product ion signal intensity. Note that as the systems get larger and the E_0 threshold values get higher (both of which are true for the $[C_6H_{11}COO^- \ H^+ \ ^-OC_6H_4pF]$ dimer), the sensitivity to multiple collision processes is enhanced especially for lower energy values. At these low collision energies, multiple collisions enhance the dissociation probability of larger complexes and those with higher critical energies more than other complexes, whereas at high energies, pressure effects are less important because dissociation of all complexes can be efficiently induced by a single collision, which is much more likely than subsequent collisions.

Double Slopes Can Be Real: The Proton Affinity of a Model Molecule

In order to better understand the origin of double slopes in the second kinetic method plots, a theoretical system was investigated. The model system was originally proposed by Drahos and Vekey [14] and also used by Ervin and Armentrout [7]. The model proton bound dimer presents 141 degrees of freedom with a mass of 243 u. The proton affinity of the unknown compound is exactly 985 kJmol^{-1} and the seven model references are molecules with identical frequencies and variable proton affinity (every 5 kJmol^{-1} from 945 to 975 kJmol^{-1}). The entropy variation between each dissociation channel is $\Delta\Delta S°_{298}$=65 Jmol^{-1}K^{-1}. In this way, perfect data with no uncertainties are obtained and the energy behavior is well defined. Figure 6 presents the first kinetic method plot obtained from ten center-of-mass kinetic energies ranging from 0.5 to 5 eV every 0.5 eV (equivalent to 3.5 to 35 eV in the laboratory frame with argon as the target gas). Note that there is extensive curvature in the lines, especially for the higher energy data. The first plot (Figure 6a) shows linear regression analyses of the data for each individual collision energy. Note that the isoequilibrium point shifts smoothly with kinetic energy. The ODR analyses of all the data (Figure 6b), of the five lowest collision energies (Figure 6c), and of the five highest collision energies (Figure 6d) are also shown [19]. It should be pointed out that the ODR plot requires the existence of an isoequilibrium point where the lines for all data cross. The ODR plot with all data included (Figure 6b) gives good agreement with the correct input values, whereas the other two analyses deviate somewhat from the correct values.

From the linear regression analyses (slopes and intercepts) of Figure 6a, data can be acquired to perform kinetic method analyses using the original extended (Figure 7a), the statistical (Figure 7c), and alternative (Figure 7d) methods. (In all cases, the data analysis is of properly weighted data. Notably, the error bars in Figure 7d are not included because they are sufficiently large to span much of the area of the plot (e.g., the lowest temperature point is T_{eff}=319±4 K and GA^{app}=964± 19 kJmol^{-1} and the highest point is T_{eff}=654±37 K and GA^{app}=945±77 kJmol^{-1}). Figure 7b also shows the value of T_{eff} as a function of the center-of-mass collision energy. Note that in the original extended plot, the data look very linear although analysis of only the low and high-energy data (five points each) yield different PA and $\Delta\Delta S°$ values. The apparent linearity is again a reflection of the cross-correlation between the GA^{app}/RT_{eff} and $1/RT_{eff}$ coordinate. In contrast, when this correlation is removed according to the statistical or alternative approaches, the plots present significant curvature. Linear fits of the low and high-energy data (five points each) yield different PA and $\Delta\Delta S°$ values, but the same values are obtained for all three approaches (as expected). In addition, these values agree approximately with the ODR results for the low and high energies (Figure 6c and d). If all the data are analyzed (resulting linear fits not shown in Figure 7), the results are again similar to those obtained with the ODR method, Figure 6b (see comparison in Table 4) although ODR yields the most accurate results compared with the input parameters. This result shows the potential of the ODR approach, which forces the lines to cross at a single point, although this approach would no longer reveal the deviations from linearity observed in the second kinetic method plots, such as those presented in Figure 2c and d.

Another interesting aspect of the ODR results in Table 4 is the very large uncertainties found for the high energy range (3–5 eV), which occurs because the branching ratios do not vary appreciably over this range. Thus, to obtain precise thermodynamic information, it is critical to include low energies (or temperatures) where the differentiation between the two product channels is maximized. This is equivalent to obtaining data in the threshold region for energy-resolved CID data.

How to Improve the Experimental Results

Various considerations may be proposed to improve the accuracy of measurements obtained by kinetic method measurements [2, 6, 7]. The quality of the references is probably the crucial point [44]. Ideally, the references should include values both above and below the molecule of interest. A series of references that are really homologous (allowing more constant $\Delta\Delta S°$ terms to be maintained) are necessary [5]. The proton affinity (or acidity) of each reference should be well defined, which should allow values of very good relative accuracy to be obtained. A series of references from which thermochemical data was obtained
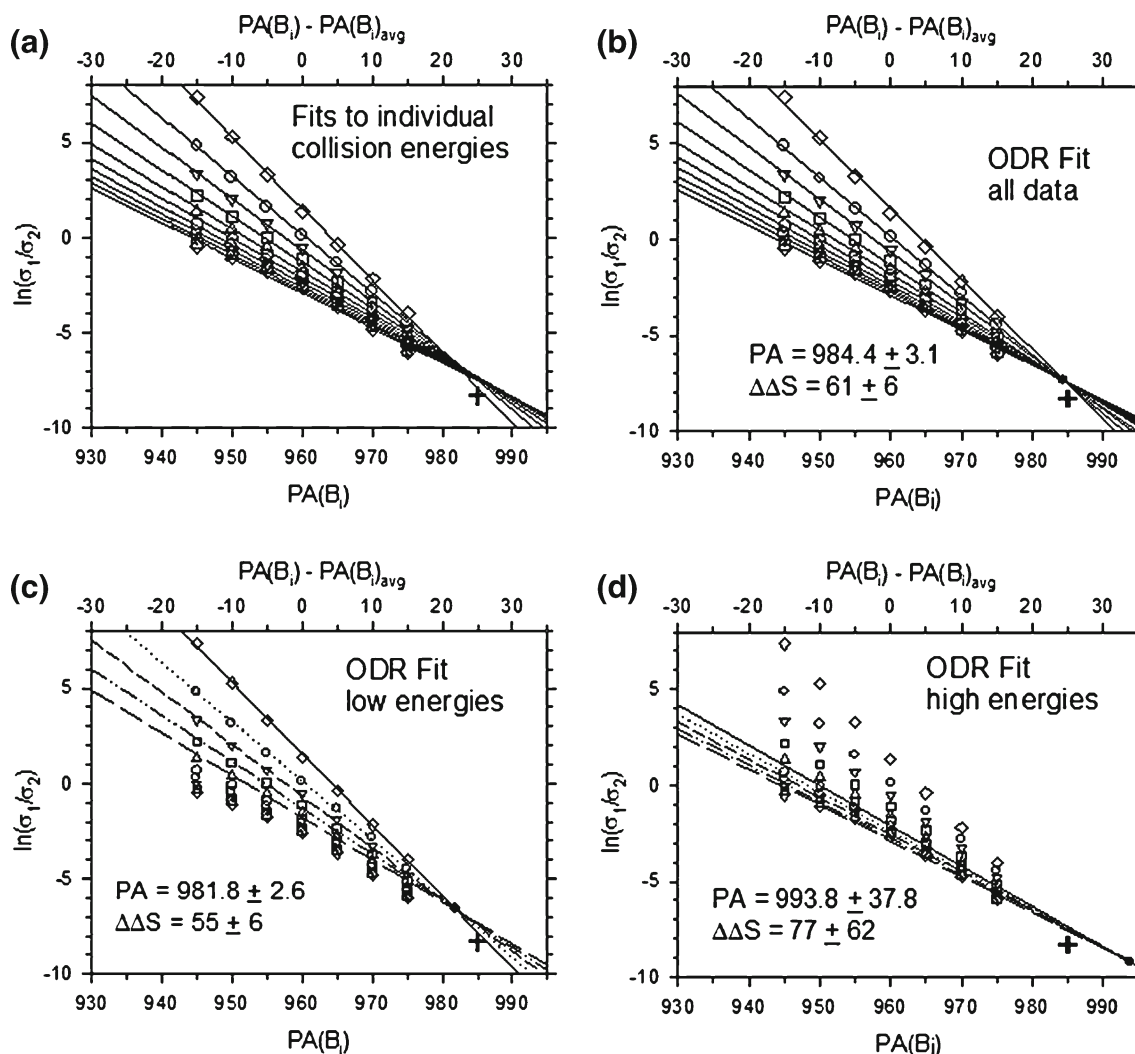
Figure 6. The logarithm of ratios of cross sections, $\ln(\sigma_1/\sigma_2)$, is plotted as a function of the reference proton affinity $PA_{298}(B_i)$ for the model system for CID at 10 relative collision energies from 0.5 (diamonds at top) to 5.0 (diamonds at bottom) eV: **(a)** linear fits to each collision energy, **(b)** orthogonal distance regression (ODR) fits of all data, **(c)** ODR fits of low energy data, and **(d)** ODR fits of high energy data. In each panel, the+symbol shows the input values of PA=985 kJmol^{-1} and $\Delta\Delta S$=65 Jmol^{-1} K^{-1}. The solid circle shows the isoequilibrium point in panels **(b)**–**(d)** for which the PA and $\Delta\Delta S$ values are provided

using the same method and from the same laboratory is preferable. This is an important point because absolute errors as reported in the NIST webbook are often in the 10–15 kJ mol^{-1} range [45]. If these errors are really random, the use of the kinetic method to acquire accurate thermochemistry is impossible because this range also corresponds to the typical maximum $\Delta H°$ difference between the reference and the compound of unknown $\Delta H°$, as illustrated in Figure 1. Larger $\Delta H°$ differences will lead to branching ratios between the two possible decomposition pathways that are too large to measure accurately. In practice, if the references are of the same origin, the relative error may be much lower, on the order of 2–5 kJ mol^{-1}. Ideally, these uncertainties should be included in the data treatment, where the relative errors are more relevant for the determination of error bars in the x axis of the first kinetic method plot. In addition, the number of references used must

be taken into consideration [46]. Three references is probably a minimum, but the use of five or more references is preferable. One advantage of using a relatively large number of references is that bad references that are uncorrelated may be more easily identified. In Figure 4, it is shown that deviation from ideal behavior is strong at low energy for cyclopentylacetic acid and at high energy for acetic acid and propionic acid, because they have the lowest E_0 values.

The use of multiple references is not always possible but increasing the effective temperature range is also in principle a good way to increase the measurement accuracy [23]. In essence, this is one fundamental reason why energy-resolved CID data is generally a superior approach to the acquisition of thermodynamic data on such systems, i.e., the data are fit over a wide range that covers the threshold (or room temperature region) to very high energies. In addition,
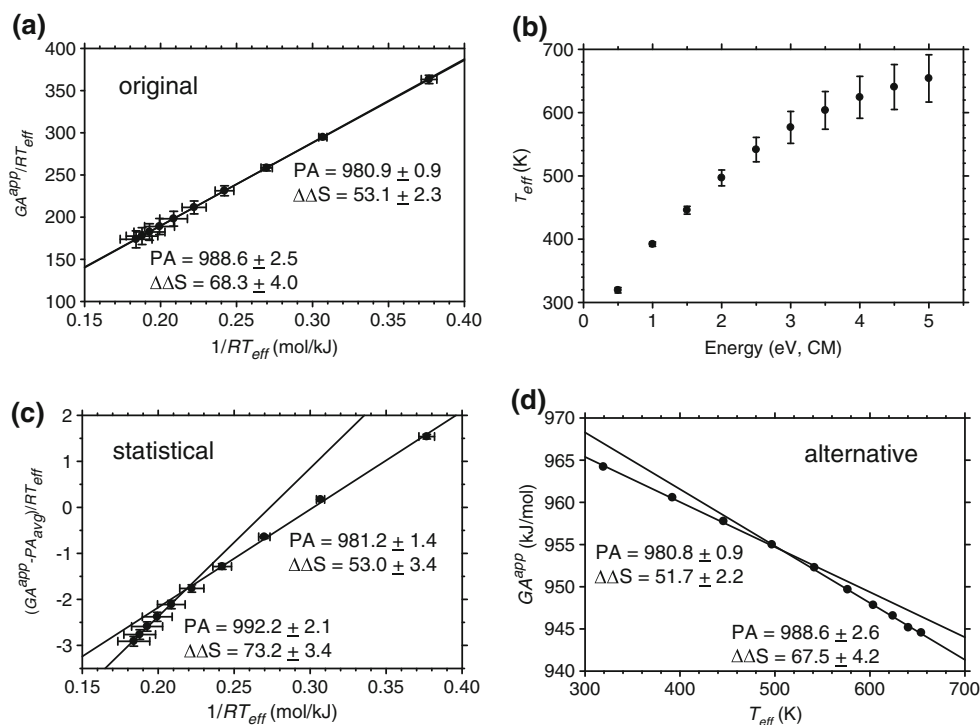
Figure 7. Extended kinetic method plots obtained from the data of Figure 6a. (a) Original extended method, (b) T_{eff} versus $E_{collision}$, (c) statistical method, and (d) alternative method. All data were generated using input values of PA=985 kJmol^{-1} and $\Delta\Delta S$=65 Jmol^{-1}K^{-1}. In parts a, c, and d, lines show weighted linear regression fits to the data at low and high energies (five points each) and the resultant PA (kJmol^{-1}) and $\Delta\Delta S$ (Jmol^{-1}K^{-1}) values obtained are shown

because these data can be modeled using a statistical approach, entropic effects are included explicitly for all individual systems, rather than forcing an average entropic factor on related but distinct systems. In such cases, establishing what data are "reliable" is more apparent, although still not foolproof. In the absence of such energy-resolved data, an efficient approach appropriate for commercial instruments is to use different instruments characterized by different time windows and yielding different kinetic shifts, as illustrated in Figure 3. For instance, a

Table 4. Data Obtained from the Theoretical Model[a]

Method	E_{coll} range (eV)	PA (kJmol^{-1})	$\Delta\Delta S°$ (Jmol^{-1}K^{-1})
Input		985	65
ODR	0.5–5.0	**984.4±3.1**	**61±6**
	0.5–2.5	981.8±2.6	55±6
	3.0–5.0	**993.8±37.8**	**77±62**
Original Extended	0.5–5.0	982.6±1.4	57.6±3.2
	0.5–2.5	980.9±0.9	53.1±2.3
	3.0–5.0	988.6±2.5	**68.3±4.0**
Statistical	0.5–5.0	982.7±1.3	56.9±3.1
	0.5–2.5	981.2±1.4	53.0±3.4
	3.0–5.0	992.2±2.1	73.2±3.4
Alternative	0.5–5.0	981.9±1.5	54.6±3.4
	0.5–2.5	980.8±0.9	51.7±2.2
	3.0–5.0	988.6±2.6	**67.5±4.2**

[a]Values within uncertainty of the input values are highlighted in bold. Uncertainties are two standard deviations in all cases.

quadrupole ion trap is characterized by a relatively long time window (1–10 ms), and therefore tends to yield decompositions under low activation conditions [47, 48]. In this case, measured T_{eff} values are close to 300 K. QQQ instruments are characterized by a time window of about 100 μs, and generally lead to higher T_{eff} values in the range of 400 to 1000 K. Although a quadrupole ion trap alone does not allow a large change in T_{eff}, together with a triple quadrupole, they offer a significant increase in the T_{eff} range [23]. Finally the data obtained on the Qq-TOF instrument are complementary as T_{eff} is in the 300–400 K range. Therefore, this instrument appears interesting in the context of the kinetic method and, in particular, together with a QQQ instrument. It should be noted that the increase of the T_{eff} range may be at the cost of the $\Delta H°$ range of references because it is important to use the same set of references with all instruments to avoid systematic errors. Thus, if the T_{eff} is too low or too high, significant changes in the branching ratio can occur, such that some references cannot be used with all instruments, as noted above for the cyclopentylacetic acid reference, which cannot be used with the ion trap or Qq-TOF instruments. Finally, it should be noted that the double slope was only clearly observed with the QQQ data because this instrument is the only one that yields a large T_{eff} range.

The use of the ODR analysis for analyzing kinetic method plots avoids correlation among derived parameters and allows all the data to be included and accurate

uncertainties to be properly evaluated. For the model system, comparison to the theoretical data demonstrates that the ODR fit (with all data) gives the most accurate determination of PA (Table 4). However, because ODR demands an isoequilibrium point, this method may hide deviations related to experimental artifacts (e.g., ion scattering and ion discrimination). The $\ln(k_i/k_0)$ versus E_{CM} plots (Figure 4) appear to be very good markers of the validity of the results (although this is most obvious when compared to the statistical analysis). Such plots were originally included in the first paper of Fenselau and coworkers on the extended kinetic method [5]. As shown by the model data in Figure 4, all the curves should tend toward a common value at high kinetic energies corresponding to the isoequilibrium point. Deviations from this ideal behavior indicate errors in the experimental data and may provide information about what energy ranges can be trusted.

Acknowledgments

References

1. Cooks, R.G., Kruger, T.L.: Intrinsic basicity determination using metastable ions. J. Am. Chem. Soc. **99**, 1279–1281 (1977)
2. Cooks, R.G., Koskinen, J.T., Thomas, P.D.: The kinetic method of making thermochemical determinations. J. Mass Spectrom. **34**, 85–92 (1999)
3. McLuckey, S.A., Cameron, D., Cooks, R.G.: Proton affinities from dissociations of proton-bound dimers. J. Am. Chem. Soc. **103**, 1313–1317 (1981)
4. Majumdar, T.K., Clairet, F., Tabet, J.C., Cooks, R.G.: Epimer distinction and structural effects on gas-phase acidities of alcohols measured using the kinetic method. J. Am. Chem. Soc. **114**, 2897–2903 (1992)
5. Cheng, X., Wu, Z., Fenselau, C.: Collision energy dependence of proton-bound dimer dissociation: entropy effects, proton affinities, and intramolecular hydrogen-bonding in protonated peptides. J. Am. Chem. Soc. **115**, 4844–4848 (1993)
6. Drahos, L., Peltz, C., Vékey, K.: Accuracy of enthalpy and entropy determination using the kinetic method: are we approaching a consensus? J. Mass Spectrom. **39**, 1016–1024 (2004)
7. Ervin, K.M., Armentrout, P.B.: Systematic and random errors in ion affinities and activation entropies from the extended kinetic method. J. Mass Spectrom. **39**, 1004–1015 (2004)
8. Nold, M.J., Cerda, B.A., Wesdemiotis, C.: Proton affinities of the N- and C-terminal segments arising upon the dissociation of the amide bond in protonated peptides. J. Am. Soc. Mass Spectrom. **10**, 1–8 (1999)
9. Vekey, K.: Internal energy effects in mass spectrometry. J. Mass Spectrom. **31**, 445–463 (1996)
10. Drahos, L., Vekey, K.: How closely related are the effective and the real temperature. J. Mass Spectrom. **34**, 79–84 (1999)
11. Wenthold, P.G.: Determination of the proton affinities of bromo- and iodoacetonitrile using the kinetic method with full entropy analysis. J. Am. Soc. Mass Spectrom. **11**, 601–605 (2000)
12. Armentrout, P.B.: Entropy measurements and the kinetic method: a statistically meaningful approach. J. Am. Soc. Mass Spectrom. **11**, 371–379 (2000)
13. Bouchoux, G., Buisson, D.-A., Bourcier, S., Sablier, M.: Application of the kinetic method to bifunctional bases ESI tandem quadrupole experiments. Int. J. Mass Spectrom. **228**, 1035–1054 (2003)
14. Drahos, L., Vekey, K.: Entropy evaluation using the kinetic method: is it feasible? J. Mass Spectrom. **38**, 1025–1042 (2003)
15. Fournier, F., Afonso, C., Fagin, A.E., Gronert, S., Tabet, J.-C.: Can cluster structure affect kinetic method measurements? The curious case of glutamic acid's gas-phase acidity. J. Am. Soc. Mass Spectrom. **19**, 1887–1896 (2008)
16. Bouchoux, G., Defaye, D., McMahon, T., Likholyot, A., Mo, O., Yanez, M.: Structural and energetic aspects of the protonation of phenol, catechol, resorcinol, and hydroquinone. Chem.–Eur. J. **8**, 2900–2909 (2002)
17. Barbour, J.B., Karty, J.M.: Resonance and field/inductive substituent effects on the gas-phase acidities of para-substituted phenols: a direct approach employing density functional theory. J. Phys. Org. Chem. **18**, 210–216 (2005)
18. Fujio, M., McIver Jr., R.T., Taft, R.W.: Effects of the acidities of phenols from specific substituent-solvent interactions. Inherent substituent parameters from gas-phase acidities. J. Am. Chem. Soc. **103**, 4017–4029 (1981)
19. Boggs, P.T., Byrd, R.H., Rogers, J.E., Schnabel, R.B.: ODRPACK Version 2.01 Software for Weighted Orthogonal Distance Regression. National Institute of Standards and Technology, Gaithersburg (1992)
20. Frisch, M.J., Trucks, G.W., Schlegel, H.B., Scuseria, G.E., Robb, M.A., Cheeseman, J.R., Zakrzewski, V.G., Montgomery, J.A., Stratmann, R.E., Burant, J.C., Dapprich, S., Millam, J.M., Daniels, A.D., Kudin, K.N., Strain, M.C., Farkas, O., Tomasi, J., Barone, V., Cossi, M., Cammi, R., Mennucci, B., Pomelli, C., Adamo, C., Clifford, S., Ochterski, J., Petersson, G.A., Ayala, P.Y., Cui, Q., Morokuma, K., Rega, N., Salvador, P., Dannenberg, J.J., Malick, D.K., Rabuck, A.D., Raghava-chari, K., Foresman, J.B., Cioslowski, J., Ortiz, J.V., Baboul, A.G., Stefanov, B.B., Liu, G., Liashenko, A., Piskorz, P., Komaromi, I., Gomperts, R., Martin, R.L., Fox, D.J., Keith, T., Al-Laham, M.A., Peng, C.Y., Nanayakkara, A., Challacombe, M., Gill, P.M.W., Johnson, B., Chen, W., Wong, M.W., Andres, J.L., Gonzalez, C., Head-Gordon, M., Replogle, E.S., Pople, J.A.: Gaussian 03. Gaussian, Inc, Pittsburgh (2002)
21. Nikolaev, E.N., Popov, I.A., Kharybin, O.N., Kononikhin, A.S., Nikolaeva, M.I., Borisov, Y.V.: In situ recognition of molecular chirality by mass spectrometry. Hydration effects on differential stability of homo- and heterochiral dimethyl tartrate clusters. Int. J. Mass Spectrom. **265**, 347–358 (2007)
22. Ma, S., Wang, F., Cooks, R.G.: Gas-phase acidity of urea. J. Mass Spectrom. **33**, 943–949 (1998)
23. Mezzache, S., Bruneleau, N., Vekey, K., Afonso, C., Karoyan, P., Fournier, F., Tabet, J.C.: Improved proton affinity measurements for proline and modified prolines using triple quadrupole and ion trap mass spectrometers. J. Mass Spectrom. **40**, 1300–1308 (2005)
24. Afonso, C., Modeste, F., Breton, P., Fournier, F., Tabet, J.C.: Proton affinities of the commonly occuring L-amino acids by using electrospray ionization-ion trap mass spectrometry. Eur. J. Mass Spectrom. **6**, 443–449 (2000)
25. Bourgoin-Voillard, S., Fournier, F., Afonso, C., Zins, E.L., Jacquot, Y., Pepe, C., Leclercq, G., Tabet, J.C.: Electronic effects of 11β substituted 17β-estradiol derivatives and instrumental effects on the relative gas phase acidity. J. Am. Soc. Mass Spectrom. **23**, 2167–2177 (2012)
26. Chernushevich, I.V.: Duty cycle improvement for a quadrupole-time-of-flight mass spectrometer and its use for precursor ion scans. Eur. J. Mass Spectrom. **6**, 471–479 (2000)
27. McMahon, T.B., Kebarle, P.: Intrinsic acidities of substituted phenols and benzoic acids determined by gas-phase proton-transfer equilibriums. J. Am. Chem. Soc. **99**, 2222–2230 (1977)
28. Lorenz, U.J., Rizzo, T.R.: Multiple isomers and protonation sites of the phenylalanine/serine dimer. J. Am. Chem. Soc. **134**, 11053–11055 (2012)
29. Jia, B., Angel, L.A., Ervin, K.M.: Threshold collision-induced dissociation of hydrogen-bonded dimers of carboxylic acids. J. Phys. Chem. A **112**, 1773–1782 (2008)
30. Ervin, K.M.: Microcanonical analysis of the kinetic method. The meaning of the "effective temperature.". Int. J. Mass Spectrom. **195/196**, 271–284 (2000)
31. March, R.E.: An introduction to quadrupole ion trap mass spectrometry. J. Mass Spectrom. **32**, 351–369 (1997)
32. Shukla, A.K., Futrell, J.H.: Tandem mass spectrometry: dissociation of ions by collisional activation. J. Mass Spectrom. **35**, 1069–1090 (2000)
33. Rodgers, M.T., Armentrout, P.B.: Statistical modeling of competitive threshold collision-induced dissociation. J. Chem. Phys. **109**, 1787–1800 (1998)

34. DeTuri, V.F., Ervin, K.M.: Competitive threshold collision-induced dissociation: gas-phase acidities and bond dissociation energies for a series of alcohols. *J. Phys. Chem. A* **103**, 6911–6920 (1999)

35. Rodgers, M.T., Ervin, K.M., Armentrout, P.B.: Statistical modeling of collision-induced dissociation thresholds. *J. Chem. Phys.* **106**, 4499–4508 (1997)

36. Armentrout, P.B., Ervin, K.M., Rodgers, M.T.: Statistical rate theory and kinetic energy-resolved ion chemistry: theory and applications. *J. Phys. Chem. A* **112**, 10071–10085 (2008)

37. Holbrook, K.A., Pilling, M.J., Robertson, S.H.: Unimolecular Reactions, 2nd ed, Wiley: Chichester (1996)

38. Gilbert, R.G., Smith, S.C.: Theory of Unimolecular and Recombination Reactions, Blackwell Scientific Publishing: Oxford (1990)

39. Pak, A., Lesage, D., Gimbert, Y., Vekey, K., Tabet, J.-C.: Internal energy distribution of peptides in electrospray ionization: ESI and collision-induced dissociation spectra calculation. *J. Mass Spectrom.* **43**, 447–455 (2008)

40. Naban-Maillet, J., Lesage, D., Bossée, A., Gimbert, Y., Sztáray, J., Vékey, K., Tabet, J.-C.: Internal energy distribution in electrospray ionization. *J. Mass Spectrom.* **40**, 1–8 (2005)

41. Muntean, F., Armentrout, P.B.: Guided ion beam study of collision-induced dissociation dynamics: integral and differential cross sections. *J. Chem. Phys.* **115**, 1213–1228 (2001)

42. Angel, L.A., Ervin, K.M.: Gas-phase acidities and O–H bond dissociation enthalpies of phenol, 3-methylphenol, 2,4,6-trimethylphenol, and ethanoic acid. *J. Phys. Chem. A* **110**, 10392–10403 (2006)

43. Armentrout, P.B.: Mass spectrometry—not just a structural tool: the use of guided ion beam tandem mass spectrometry to determine thermochemistry. *J. Am. Soc. Mass Spectrom.* **13**, 419–434 (2002)

44. Cooks, R.G., Patrick, J.S., Kotiaho, T., McLuckey, S.A.: Thermochemical determinations by the kinetic method. *Mass Spectrom. Rev.* **13**, 287–339 (1994)

45. Linstrom, P.J., Mallard, W.G.: In: National Institute of Standards and Technology, Gaithersburg MD, 20899. Available at: http://webbook.nist.gov (2005)

46. Bouchoux, G.: Evaluation of the protonation thermochemistry obtained by the extended kinetic method. *J. Mass Spectrom.* **41**, 1006–1013 (2006)

47. Remes, P.M., Glish, G.L.: On The time scale of internal energy relaxation of AP-MALDI and nano-ESI ions in a quadrupole ion trap. *J. Am. Soc. Mass Spectrom.* **20**, 1801–1812 (2009)

48. Afonso, C., Lesage, D., Fournier, F., Mancel, V., Tabet, J.-C.: Origin of enantioselective reduction of quaternary copper d, l amino acid complexes under vibrational activation conditions. *Int. J. Mass Spectrom.* **312**, 185–194 (2012)

49. Caldwell, G.W., Renneboog, R., Kebarle, P.: Gas-phase acidities of aliphatic carboxylic acids, based on measurements of proton-transfer equilibria. *Can. J. Chem.* **67**, 611–618 (1989)

50. Graul, S.T., Schnute, M.E., Squires, R.R.: Gas-phase acidities of carboxylic acids and alcohols from collision-induced dissociation of dimer cluster ions. *Int. J. Mass Spectrom. Ion Process.* **96**, 181–198 (1990)